Minerals Engineering 130 (2019) 57–66

Contents lists available at ScienceDirect

Minerals Engineering

journal homepage: www.elsevier.com/locate/mineng

Coupling comminution indices and mineralogical features as an approach to a geometallurgical characterization of a copper ore

Jonathan Rincon[a,*], Stoyan Gaydardzhiev[a], Lachezar Stamenov[b]

[a] University of Liège, GeMMe, Laboratory of Minerals Engineering and Recycling, Sart-Tilman Campus-B52, 4000 Liège, Belgium
[b] Dundee Precious Metals Chelopech, 2087 Village of Chelopech, Bulgaria

ARTICLE INFO

Keywords:
Geometallurgy
Comminution
Impact breakage
Work index
Process mineralogy
Principal component analysis

ABSTRACT

A production block of the underground mine exploiting the Chelopech high sulphidation epithermal copper-gold deposit was subjected to geometallurgical modelling. This study details the procedure used based on traditional comminution and mineralogical indices. Drop weight and batch grinding tests were performed on representative samples to yield parameters related to Axb and operating work OWi indices. These were further correlated with the ore mineralogical features using principal component analysis. Modal mineralogy data processed by a set of linear equations enabled the estimation of the aforementioned indices with a deviation of ± 2.4 for Axb and ± 9.08 kWh/t for OWi respectively. Based on ore textural characteristics and non-sulphide gangue (NSG) minerals content, two geometallurgical domains were identified as a first approach to modelling of the studied block.

1. Introduction

The mining industry is witnessing a constant decline of metal values in new mineral deposits discoveries (Baum, 2014; Lishchuk, 2016; Lishchuk et al., 2015). In response, deeper and more complex geological settings have stimulated research centres and mining companies to work together in order to better control mining schedule by reducing uncertainty, risk and to increase cost efficiency (Cropp et al., 2014; Walters, 2009; Wills and Finch, 2016). Geometallurgy has been regarded as a new discipline with capabilities of forecasting production and economic variables. Geological, metallurgical and mining properties are combined, providing an efficient tool for optimized resource management (Bradshaw, 2014; Lund and Lamberg, 2014; Walters, 2009; Zhou and Gu, 2016). As a result, traditional block models based solely on element head grades have been fed with data on mineral distributions, petrophysical properties, estimated grade – recovery or work indices, among others (Lishchuk et al., 2015). Several examples on the advantages of using geometallurgy can be found in the literature (Evans et al., 2011; Lopera Montoya, 2014; Lotter, 2011; Suazo et al., 2010; Tungpalan et al., 2015; Vizcarra et al., 2010), where challenges associated with flotation underperformance, comminution energy optimization, production forecasting or flowsheet design have been overcome by using modelling and simulation tools based on mineral features such as mineral composition, grain size, associations or liberation degree.

Dundee Precious Metals (DPM) is a Canadian-based company active in extraction and production of commodities such as copper and gold. DPM's flagship operation is located in Chelopech, Bulgaria; an underground mine which produces copper and pyrite concentrates. The mine started operation in 1954, with an expansion in 1975 to being further acquired by DPM in 2004. Crushed ore is processed through a flotation circuit fed from a SAG mill. Copper bearing minerals and pyrite are concentrated to deliver grades of 15–17% copper, 20–30 g/t gold and 5% arsenic on average.

The company brought into exploitation a block which has not been included in the mining program schedule so far. Due to the high geological and mineralogical complexity, a geometallurgical oriented study of the block was proposed with the aim to predict ore behaviour in comminution and flotation. More precisely, the study encompasses characterization of feed and products from a laboratory bulk sulphide flotation, single particle impact breakage and batch grinding tests. With the aim to create mineral based models able to predict variables such as flotation recovery, operating work index (*OWi*) and *Axb* index inside the block, quantification of mineral features was correlated to the measured data. The present paper reports on the results from the impact breakage and grinding studies.

2. Materials and methods

A geometallurgical modelling methodology developed by

* Corresponding author.
E-mail address: jjgamero@uliege.be (J. Rincon).

https://doi.org/10.1016/j.mineng.2018.10.007
Received 30 January 2018; Received in revised form 10 September 2018; Accepted 8 October 2018

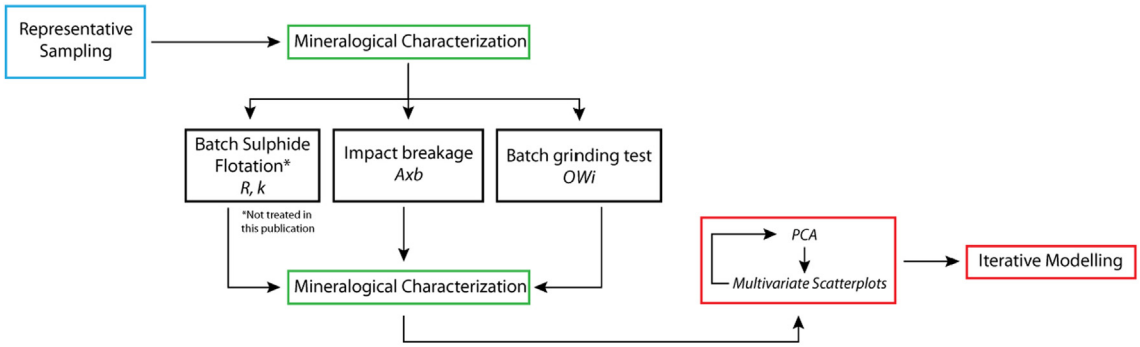

Fig. 1. Conceptual pattern of the geometallurgical characterization (adapted from Keeney, 2010).

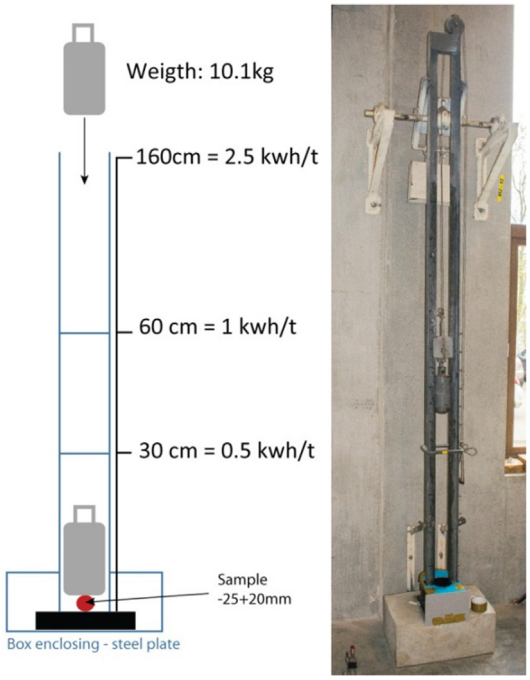

Fig. 2. Drop weight test set up used for the experiments.

researchers at the Julius Kruttschnitt Mineral Research Centre – JKMRC (Keeney, 2010; Keeney and Walters, 2009; Lopera Montoya, 2014; Tungpalan et al., 2015; Vatandoost et al., 2009) was adapted with its flowsheet pattern shown in Fig. 1.

In order to identify the main minerals influencing comminution performance, mineral characteristics and metallurgical variables were correlated using principal component analysis (PCA). Due to the limited amount of samples and high amount of variables, PCA was considered a practical method to find correlations between the target variables in different variability dimensions or factorial planes. The data set used in the PCA was comprised of the mineral composition of 9 ore samples and one measured comminution index (*Axb* or *OWi*). Once mineralogical variables that better correlated with a specific metallurgical variable were identified, linear equations were created by iterative modelling.

The iterative procedure serving to support the linear regression between the metallurgical variables (Y) and mineral variable (X) was done following the equation (1).

$$Y' = mX + d \tag{1}$$

Further on, the difference between the estimated variables (Y′) and the experimental ones (Y) was correlated against new mineralogical variables (Z) to obtain new estimations (Y″) as shown in Eq. (2). The process was finalized when the minimum root mean square error (RMSE) and maximum coefficient of determination (R2) were achieved after data cross-validation (Y vs. Y′).

$$Y'' = mX + cZ + d \tag{2}$$

2.1. Sample preparation

Drill core samples and hand-picked specimens were collected by the geological team of DPM Chelopech at 9 different locations within the block. Each sample collected was approx. 10 kg keeping representativeness in terms of Cu grade, texture, mineralization style and lithology. The drop weight tests required approx. 2 kg of material. Drill core fragments of about 10 cm in length were crushed using a rock hammer and sieved at 25 and 20 mm to ultimately obtain 90 pieces in the size rage of −25 + 20 mm. As a rule, for performing a complete JK-Drop weight test (Lynch et al., 2015; Napier-Munn et al., 1996) five size classes need to be tested. However, due to the exploratory character of the study, only one size class and three specific energy levels were performed. 3 batches of 30 fragments were prepared for each sample available.

An additional 2.5 kg of each sample was crushed in a jaw crusher to 99% passing 3.35 mm. This material served as feed for the batch grinding tests with particle size distribution (PSD) estimated by sieving through the following screens (mm): 3.35, 2.36, 1.18, 0.84, 0.425, 0.3, 0.212, 0.15, 0.075 and 0.053.

2.2. Drop weight test methodology

The conceptual design of the adapted JKMRC drop weight test (JK-DWT) is presented in Fig. 2. The test was performed on a 3 m steel structure enabling a weight of 10.1 kg to be dropped down from three defined heights of 30, 60 and 160 cm, respectively corresponding to three specific energies of 0.5, 1 and 2.5 kWh/t.

The specific energy applied to each sample at the different heights was calculated using Eq. (3) (Napier-Munn et al., 1996),

$$Ecs = \frac{(h * M_w * 0.0272)}{Mp} \tag{3}$$

where

Ecs – specific energy (kWh/t)
h - drop height, (cm)
Mw - mass of the weight, (g)
Mp - average mass of each particle, (g)

Depending on the type of ore sample (i.e., Mp), the actual applied energies deviated slightly from the ones calculated based on Eq. (3). Therefore, the specific energy values were corrected and are displayed in Table 1.

The fractions obtained from each energy test (3 products per ore sample) were dry sieved on screens with the following openings (mm): 20, 12.5, 7.92, 5.66, 3.35, 2.36, 1.18, 0.84, 0.42, 0.3, 0.21, 0.15, 0.075

Table 1
Corrected specific energies applied to each sample. Calibration was performed using Eq. (3) and the weights of each sample.

Sample ID	Corrected energy (kWh/t)	Sample ID	Corrected energy (kWh/t)	Sample ID	Corrected energy (kWh/t)
Sample 2	2.6	Sample 5	2.5	Sample 8	2.7
	1.0		0.9		1.0
	0.5		0.5		0.5
Sample 3	2.4	Sample 6	2.4	Sample 9	2.3
	0.9		0.9		0.9
	0.5		0.5		0.4
Sample 4	2.7	Sample 7	2.8	Sample 10	2.8
	1.0		1.0		1.0
	0.5		0.5		0.5

and 0.053. Non-cumulative retained PSD were plotted in order to estimate in which size ranges the samples deviated the most. Representative samples were sent for mineralogical quantification through X-ray powder diffraction (XRD).

The relationship between *Ecs* and t_{10} (proportion of mass under one tenth of the original particle mean size; in this case 2.236 mm) is given by Eq. (4) (Lynch et al., 2015; Napier-Munn et al., 1996),

$$t_{10} = A*[1-e^{(-b*E_{cs})}] \quad (4)$$

where *A* and *b* are the parameters that describe the Ecs vs. t_{10} curve. It should be noted that *A* and *b* parameters vary depending on the type of material. The parameter *A* is the maximum t_{10}, i.e. sill of the curve and *b* governs slope/rate of increase of t_{10}.

A comparison between the 9 ore samples subjected to the tests was performed by ranking them based on the *Axb* index, thus enabling the assessment of ore resistance to impact breakage. *Axb* is an important parameter used in SAG mills design and hence it has high relevance to the study (Bueno et al., 2013; Lynch et al., 2015; Magalhães and Tavares, 2014; Napier-Munn et al., 1996). A total of 810 drops were conducted for the nine samples studied; thirty drops per energy yielding ninety drops per sample.

2.3. Grindability

Grindability was assessed using a Magotteaux laboratory ball mill. For each test, 1000 cm^3 of solids at 99% passing 3.35 mm were placed inside the mill, and then 1850 cm^3 of water was added to give a pulp density of ca. 51 %wt. The mill was charged with 20 kg of 30 mm diameter forged steel balls and run at 65 rpm with duration of 5.30 min. Once both feed and products were sieved, the operating work index (OWi) was calculated using Eq. (5) shown below (Keeney, 2010; Michaux and Kojovic, 2008).

$$OWi = \frac{W}{10*\left(\frac{1}{\sqrt{P}}-\frac{1}{\sqrt{F}}\right)} \quad (5)$$

where

F: 80% passing feed size
P: 80% passing product size
W: (A* number of revolutions of the ball mill)/sample mass (kg)
A: calibration constant.

The index corresponds to an empirical equation designed for Bond Ball Mill Work Index (BMWi) prediction. The calibration constant A corresponds to a number in kWh*kg/t, whose value represents specific energy correlations between this procedure and the original Bond work index test procedure (Michaux and Kojovic, 2008). As the dimensions of the Magotteaux mill are different to those of a conventional Bond mill (30 × 30 cm), the obtained data on *OWi* (kWh/t) was used merely for the sake of ranking the ore resistance to grinding. Non-cumulative retained PSD in percentage was plotted for grinding products with the objective of identifying the size classes in which the samples deviated the most.

2.4. Mineralogical characterization

The ore samples were characterized prior and after the comminution tests. Modal mineralogy, texture, associations, alterations and grain sizes were examined on representative polished blocks and grain mounts. XRD was performed using a Bruker D8-ECO powder X-ray diffractometer with CuKα radiation. The quantification was done using the Rietveld refinement which models the powder patterns starting from the crystal structure of the different phases (Bish and Plötze, 2011). Based on the particle size distribution of the test products, the size classes where peaks of mass distribution were identified and where sample variability was significant were selected as sampling points.

Around 5 g of material previously ground at 80% passing 90 μm were used to fabricate grain mounts with 30 mm diameter, following an established procedure (Bouzahzah et al., 2015). The resin grain mounts were introduced into a ZEISS Gemini Sigma 300 system coupled with two Bruker xFlash 6|30 x-ray detectors and processed by ZEISS Mineralogic Mining Automated Mineralogy. The analyses were carried out using a current of 167 μA with an acceleration voltage of 20 kV. Quantitative mineralogical features were measured in a recipe-oriented protocol. The process consisted of a complete sample mapping by setting an analysis grid of 3 μm step size at 2600× magnification applied to sampling fields of 10 × 10 mm per sample. The dwell time was 0.075 s and after measurement of 15,000 particles, the analysis was terminated (Graham et al., 2015).

BSE images of 3000 × 2000 pixels were used during post processing of the X-ray spectra. Erosion, dilation, and thresholding were implemented in a pre-defined order to be able to classify the pixels in the images (i.e. segmentation) and produce an additional output consisting of mineral maps of the samples. The minerals were classified according to their average elemental compositions and additional constraints to not measure grains touching borders inside sampling fields and to neglect grains smaller than 5 μm were imposed. In addition, the polished blocks were characterized using an OLYMPUS BX60 reflected light optical microscope to identify textural characteristics.

3. Results and discussions

3.1. Comminution related features

3.1.1. Drop weight test

The particle size distribution at each energy level per sample is plotted in Fig. 3. The curves suggest that all samples follow the same trend of peaks and valleys; however there are some differences between them, especially at the lowest specific energy range. It should be noted that at energy of 1 kWh/t, the samples present high PSD variability and low variability among the actual specific energy values applied (Table 1). For particles smaller than 1 mm, the impact breakage reduces its efficiency as the yield of finer size fractions does not increase as much as for those coarser than 1 mm. It can be seen also, that the majority of size reduction effects took place at around 10 mm. Therefore, samples from the 1 kWh/t products are taken from −12.5 + 7.925 and −1.18 + 0.840 mm size classes (Fig. 3).

One could note in Fig. 4, that all samples present different response at the *t10* vs. *Ecs* curve. Sample 10 (S10) present the most significant response, followed by S8, whereas S6 exhibits the lowest one. The calculated *Axb* values implying the higher the *Axb* value the less ore resistance are shown in Table 2. S10 and S8 present the highest *Axb* with values of 37.25 and 36.63 respectively, whilst S3 and S6 show the lowest values of 22.80 and 21.30. These latter can be considered as the

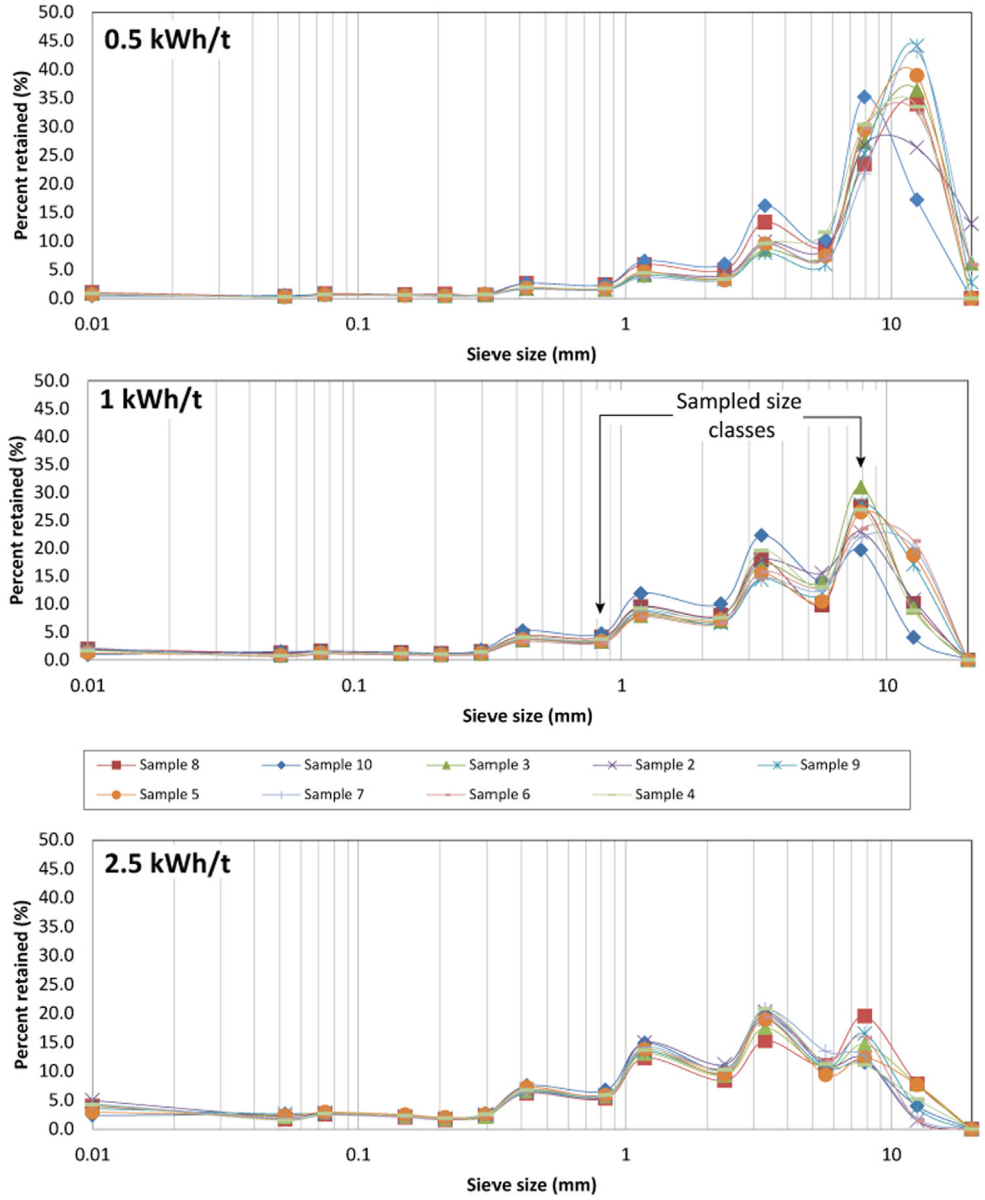

Fig. 3. Single particle size distributions of drop weight tests products.

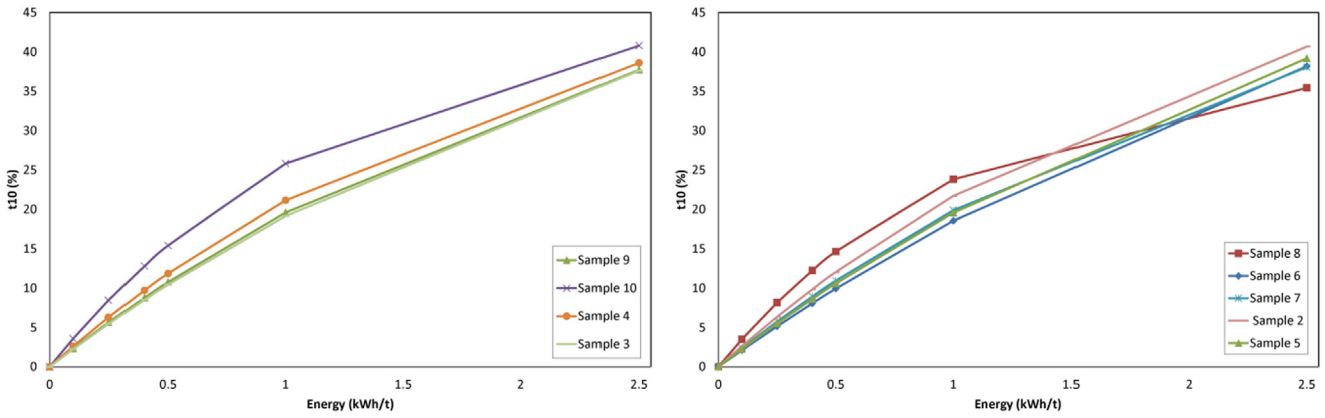

Fig. 4. Specific energy vs. t10 for the 9 samples. Curves are grouped according to samples' mineralization style - stockwork (left) and disseminated sulphides (right).

Table 2
Samples summary for the drop weight and batch grinding tests.

Sample ID	Type of material	Lithology	Mineralization style	Axb	OWi (kWh/t)
Sample 2	Half drill cores	Brecciated tuff	Disseminated sulphides	26.84	9.34
Sample 3	Half drill cores	Brecciated tuff	Stockwork	22.80	9.92
Sample 4	Half drill cores	Brecciated tuff	Stockwork	26.72	10.18
Sample 5	Half drill cores	Brecciated tuff	Disseminated sulphides	22.95	11.85
Sample 6	Half drill cores	Brecciated tuff	Disseminated sulphides	21.30	10.88
Sample 7	Chips	Brecciated tuff	Disseminated sulphides	24.16	9.05
Sample 8	Chips	Brecciated tuff	Disseminated sulphides	36.63	10.42
Sample 9	Half drill cores	Brecciated tuff	Stockwork	23.70	9.52
Sample 10	Chips	Brecciated tuff	Stockwork	37.25	14.89

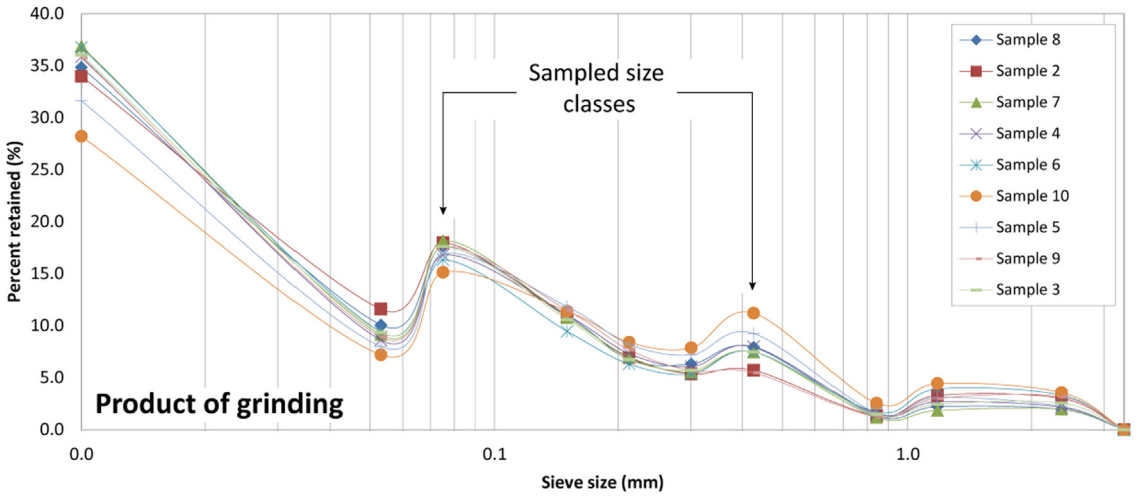

Fig. 5. Single particle size distribution from batch grinding tests.

most resistant against impact breakage (the hardest) among the 9 samples being tested.

3.1.2. Grindability

The calculated values of *OWi* are shown in Table 2. These results rank the samples according to their resistance to comminution experienced inside the ball mill, i.e. from hardest to weakest ore. It can be noted that S10, S5 and S6 show the three highest *OWi* values with 14.9, 11.9 and 10.9 kWh/t respectively. On the other hand, S7, S2 and S9 present an *OWi* of 9.1, 9.3 and 9.5 kWh/t. From the particle size distribution presented in Fig. 5 it is noted that the 0.425 mm and 0.075 mm regions on the curves show the most variability between samples. Therefore, mineralogical characterization was performed on samples taken in the −0.840 + 0.425 mm and −0.150 + 0.075 mm size range.

3.2. Mineralogical features

Breccia and tuff are regarded as the predominant texture of the samples hosting the ore mineralization, which is presented in the form of disseminated sulphides and stockwork veins types. Breccia textures result from tectonic and/or magmatic events, forming tectonic or hydraulic breccia. This texture was identified in virtually all the samples from both the drill cores and hand specimen (Fig. 6).

Stockwork is the predominant mineralization style identified in samples S9, S10, S4 and S3 (Table 2). It is characterized by sulphide veins intruding the brecciated tuff matrix. Common mineral associations in these textures include pyrite interlocked with tennantite, enargite and chalcopyrite (Fig. 6). The veins can present widths with thickness of about 10–20 µm to 1 cm. The contact between veins and host rock is gradual to sharp.

Disseminated sulphides are the predominant mineralization style in S5, S7, S2, S6, and S8 (Table 2). They are characterized by scattered sulphide grains hosted in tuff or brecciated tuff matrix. Pyrite, enargite, tennantite and chalcopyrite are present in binary, ternary and more complex associations (Fig. 6). Other identified textures included massive and replacements between sulphide minerals. Replacement textures are common between chalcopyrite, pyrite and tennantite (Fig. 6).

The results from the automated mineralogy for the feed samples of the comminution tests are shown in Fig. 7. Quartz, pyrite, kaolinite and dickite are the most common mineral phases representing more than 95 %wt. of the mineral content. Quartz content varied from 38.3 to 63.8 %wt., pyrite is between 15.1 and 34.7 %wt. and kaolinite + dickite between 6.1 and 25.3 %wt. The sulphosalts group (luzonite, tennantite, enargite) is the most common copper bearing phase among all the samples with values between 0.8 and 3.4 %wt., followed by chalcopyrite present in a range between 0.3 and 2.1 %wt.

The mineralogical assay on the products taken from the samples subjected to 1 kWh/t impact energy, identified quartz as the most common mineral in all the samples, followed by kaolinite + dickite and pyrite.

Table 3 presents the mineral composition of the 9 products sampled in the size classes −12.50 + 7.93 mm and −1.18 + 0.840 mm. When normalizing these results to feed mineralogy in the −1.18 + 0.840 mm class, it is possible to notice that the mineralogical composition of the material retained in the size fractions strongly differs from that of the feed (Fig. 8). It is noticeable in Fig. 8 that quartz and pyrite contents are the ones that resemble the most to the feed presenting differences in the range of ± 0.5. On the other hand, kaolinite + dickite normalized content is the one differing the most with values between 0.6 and 2.8, followed by sulphosalt values in the range between 0.0 and 0.8.

On the other side, XRD results from the batch grinding tests for −0.150 + 0.075 mm and −0.840 + 0.425 mm are presented in Table 4. Likewise DWT results, quartz, kaolinite + dickite and pyrite

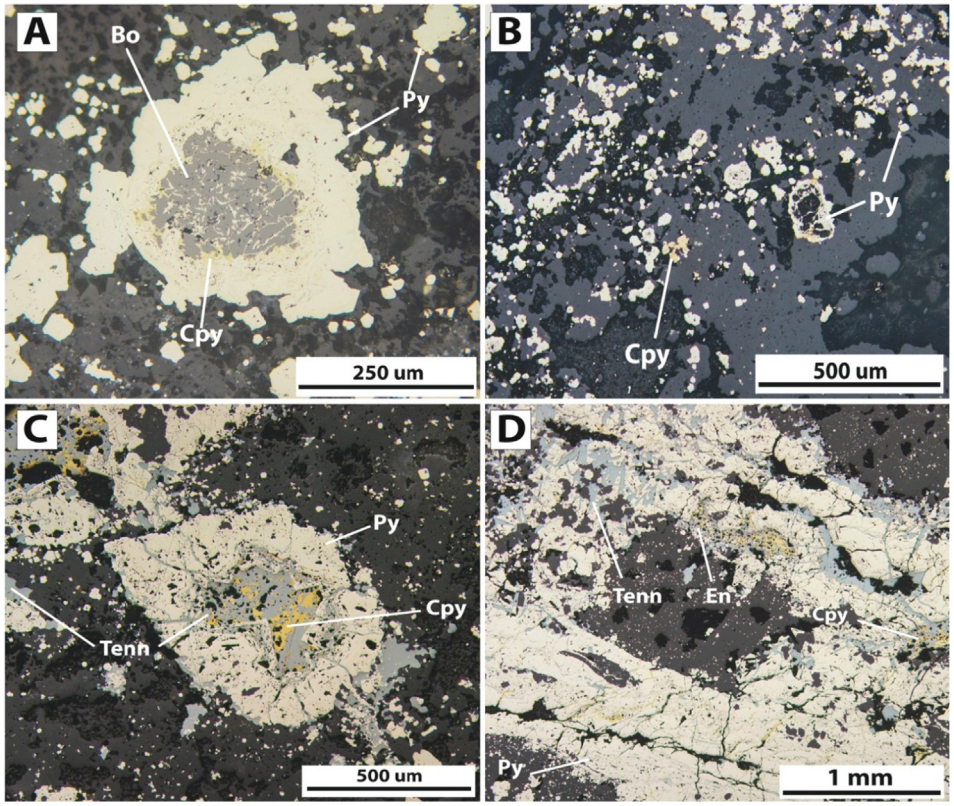

Fig. 6. A Bornite replacing pyrite and chalcopyrite in S7. B - Disseminated texture of pyrite crystals and skeletal pyrite observed in S5. C - Pyrite aggregate in association with tennantite and chalcopyrite, tennantite fills fractures in pyrite resembling vein related textures in S3. D - Tennantite, enargite and chalcopyrite in association with pyrite. Bo: Bornite, Py: Pyrite, Cpy: Chalcopyrite, Tenn: Tennantite, En: Enargite.

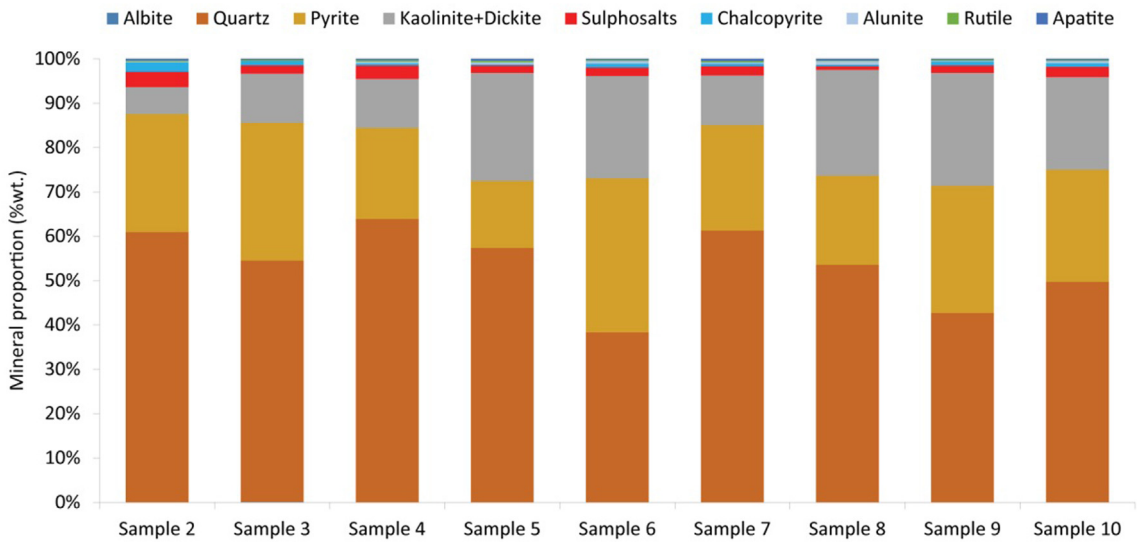

Fig. 7. Modal mineralogy of the 9 samples used.

are the most common minerals, and normalization of the quartz, kaolinite + dickite, pyrite and sulphosalts contents in the −0.150 + 0.075 mm size class is presented in Fig. 9. It is appreciable that quartz normalized content is the one closer to the feed, with values between 1.0 and 1.3. Differently, pyrite values are below 1 which implies that its concentration is less in the sampled size fractions than in the feed (Fig. 9). Finally, sulphosalts and kaolinite + dickite values are between 0.1 and 1.4, and 0.7 and 2.2 respectively, presenting the highest difference in content from the sampled size classes to feed.

In general, there is an overlap between the results presented in Figs. 8 and 9. From both figures it can be noticed that the samples presented the same compositional relationships of size fractions to the feed in both comminution tests, where there are samples that accumulated twice as much kaolinite + dickite (and 0.5 times less sulphosalts) in both size fractions. In addition, there is no preference to any mineralization style, as samples from both textural classifications overlapped in these results. Nevertheless, it can be stated that under DWT/grinding conditions, kaolinite group minerals preferentially compose the fine size fractions.

3.3. Correlating modal mineralogy and comminution indices

The drop weight test (DWT) results suggest that the *Axb* index can be used to rank the ore resistance to impact breakage. When *Axb* indices are correlated to the amount of kaolinite + dickite, one could infer that the higher the content of these minerals in the −1.18 + 0.840 mm

Table 3
Mineral composition of drop weight tests products in size classes −1.18 + 0.840 mm and −12.5 + 7.925 mm.

Sample ID	Size class	Py (%wt.)	Cpy (%wt.)	E + T (%wt.)	K + D (%wt.)	Qtz (%wt.)	Ab (%wt.)	TOTAL (%wt.)
Sample 2	−1.18 + 0.84 mm	31.4	1.3	2.7	15.7	47.7	1.1	100.0
Sample 3		18.6	0.5	0.9	26.7	52.1	1.2	100.0
Sample 4		11.8	0.5	1.8	24.3	60.1	1.5	100.0
Sample 5		8.4	0.2	0.8	27.9	61.5	1.2	100.0
Sample 6		22.8	0.2	0.4	29.6	46.1	1.0	100.0
Sample 7		11.1	1.7	0.9	32.2	52.7	1.4	100.0
Sample 8		17.1	1.4	0.0	15.5	66.0	0.0	100.0
Sample 9		10.1	0.1	0.1	28.4	59.5	1.8	100.0
Sample 10		17.6	0.9	1.5	16.6	62.7	0.7	100.0
Sample 2	−12.5 + 7.93 mm	17.9	0.9	2.5	21.6	55.7	1.4	100.0
Sample 3		9.8	0.3	0.5	39.8	48.5	1.1	100.0
Sample 4		12.5	0.3	2.3	22.2	61.1	1.6	100.0
Sample 5		7.4	0.4	2.7	29.8	58.6	1.2	100.0
Sample 6		26.1	0.1	0.3	32.5	39.5	1.5	100.0
Sample 7		10.2	1.9	1.1	36.4	49.1	1.2	100.0
Sample 8		9.7	1.1	0.0	24.7	64.6	0.0	100.0
Sample 9		8.7	0.2	0.3	34.5	55.1	1.2	100.0
Sample 10		19.1	2.0	2.8	21.5	54.5	0.2	100.0

Py: pyrite, Cpy: Chalcopyrite, E: enargite, T: tennantite, K: kaolinite, D: dickite, Qtz: Quartz, Ab: Albite.

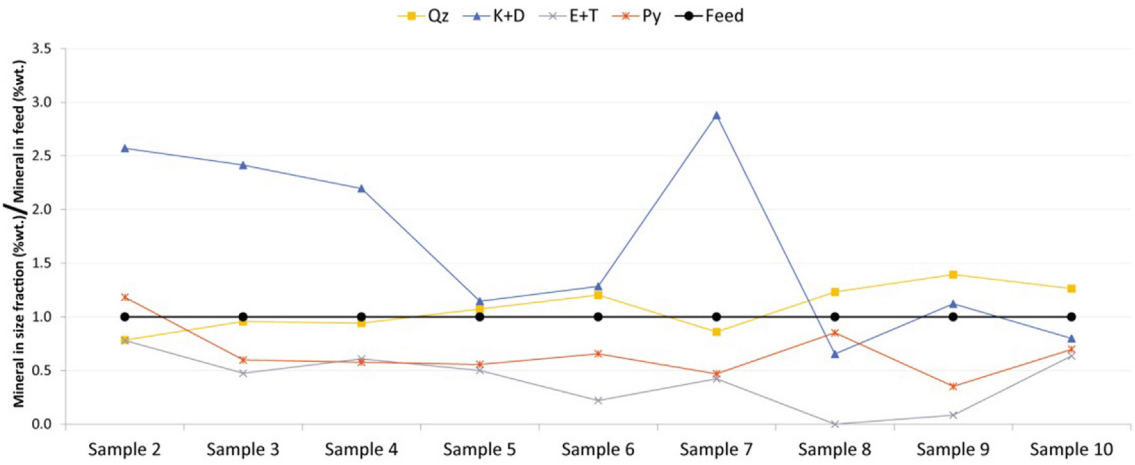

Fig. 8. Quartz (Qz), kaolinite + dickite (K + D), sulphosalts (E + T) and pyrite (Py) contents in %wt. for DWT products in the size fraction −1.18 + 0.840 mm normalized to feed content.

Table 4
Mineral composition of products from batch grinding tests belonging to size classes −0.150 + 0.075 mm and −12.5 + 7.925 mm.

Sample ID	Size class	Py (%wt.)	Cpy (%wt.)	E + T (%wt.)	K + D (%wt.)	Qtz (%wt.)	Ab (%wt.)	TOTAL (%wt.)
Sample 2	−0.150 + 0.075 mm	21.1	1.3	1.4	13.7	61.2	1.2	100.0
Sample 3		20.0	0.4	0.7	20.5	56.9	1.4	100.0
Sample 4		12.5	0.4	2.3	22.0	61.4	1.4	100.0
Sample 5		10.8	0.9	2.3	21.6	62.2	2.3	100.0
Sample 6		31.3	0.4	0.8	16.2	50.3	1.0	100.0
Sample 7		16.6	1.2	0.7	18.9	59.1	3.4	100.0
Sample 8		13.4	0.6	0.1	18.2	66.3	1.4	100.0
Sample 9		19.7	0.7	0.9	17.7	57.6	3.4	100.0
Sample 10		15.9	0.3	0.2	18.4	63.2	1.9	100.0
Sample 2	−0.840 + 0.425 mm	19.9	0.9	1.0	12.4	64.3	1.5	100.0
Sample 3		9.4	0.2	0.4	26.3	62.1	1.6	100.0
Sample 4		9.0	0.2	1.3	27.5	60.7	1.3	100.0
Sample 5		6.0	0.4	1.0	29.6	61.7	1.4	100.0
Sample 6		25.1	0.4	0.8	18.8	54.0	0.9	100.0
Sample 7		11.8	0.7	0.0	23.3	63.2	1.0	100.0
Sample 8		5.8	0.3	0.0	26.8	65.9	1.1	100.0
Sample 9		17.8	0.3	0.6	17.7	62.2	1.4	100.0
Sample 10		9.8	0.2	0.0	19.9	69.1	1.1	100.0

Py: pyrite, Cpy: Chalcopyrite, E: enargite, T: tennantite, K: kaolinite, D: dickite, Qtz: Quartz, Ab: Albite.

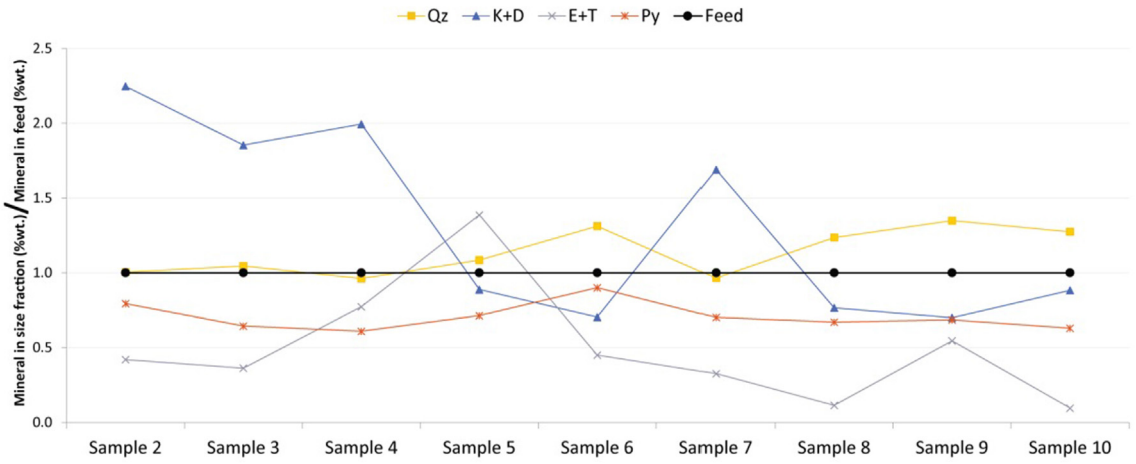

Fig. 9. Quartz (Qz), kaolinite + dickite (K + D), sulphosalts (E + T) and pyrite (Py) contents in %wt. for grinding products in the size fraction −0.150 + 0.075 mm normalized to feed content.

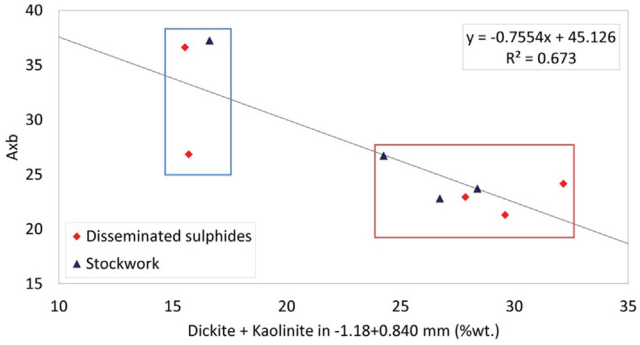

Fig. 10. Axb index calculated for the 9 samples as a function of dickite + kaolinite content in the −1.18 + 0.840 mm size class.

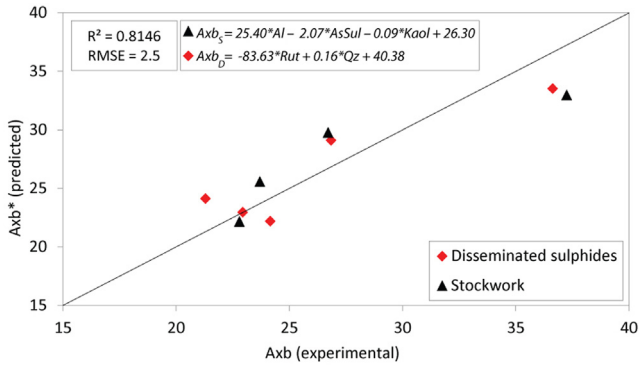

Fig. 11. Comparison between predicted and experimental Axb indices. Al: Alunite, AsSul: Sulphosalts, Kaol: Kaolinite + Dickite, Rut: Rutile, Qz: Quartz.

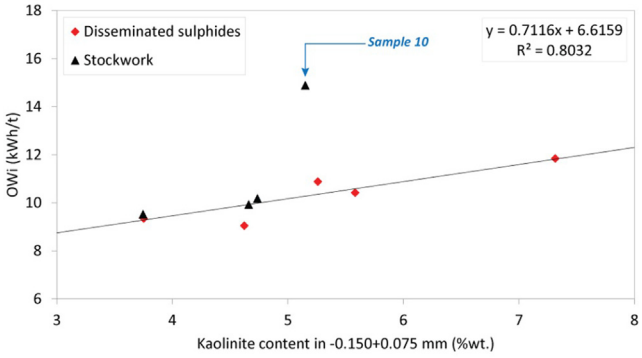

Fig. 12. Operating work index (OWi) as a function of kaolinite content in −0.150 + 0.075 mm size class.

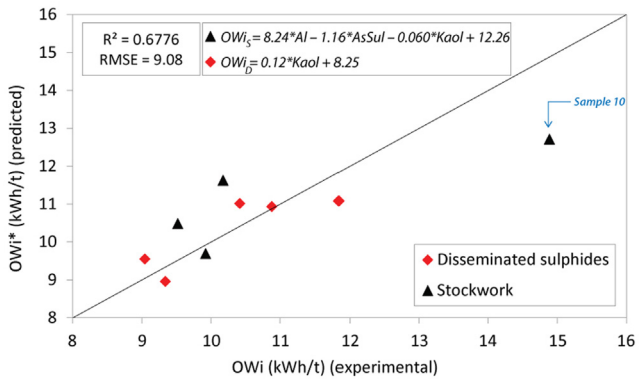

Fig. 13. Comparison predicted and experimental *OWi* indices. Al: Alunite, AsSul: Sulphosalts, Kaol: Kaolinite + Dickite.

class, the lower the *Axb* index (Fig. 10). However, when correlating the kaolinite content in the feed samples to *Axb*, it is not possible to find any sort of correlation as in Fig. 10. These results may be attributed to the possibility of kaolinite + dickite content in the analysed size fraction explaining solely the variation in *Axb* values from sample to sample; whereas, *Axb* correlation to the feed, may need additional minerals.

Koncagül and Santi (1999) showed that kaolinite content can increase uniaxial compressive strength in rocks; however it can decrease their durability because these rocks tend to slake due to pore air compression. In other words, a strong rock not necessarily means a durable one, the higher the amount of these minerals the lower the rock abrasion hardness (Conca and Rossman, 1985). Furthermore, the Chelopech deposit is classified as a high-sulphidation epithermal in which the mineralization of the studied block is mostly present within the denominated silica halo, at the boundary with advanced argillic alteration, where kaolinite and dickite originated as products of the hydrothermal alteration of Al_2O_3, SiO_2, K_2O, Na_2O bearing minerals. Accordingly, the hypothesis behind this behaviour is that the association in the parental rock of kaolinite group minerals with the other rock forming minerals may impede high values of t_{10} in the impact breakage products. The results shown in Fig. 10 also suggest that the mineralization style do not influence ore behaviour under breakage, as both disseminated sulphides and stockwork follow the linear trend. However, the fact that three of the samples (blue box) are positioned aside

from the main group (red box), could imply that other mineral occurrences might control the breakage behaviour as well.

The PCA realized through correlation between the *Axb* indices and feed's modal mineralogy, suggest that besides the content of kaolinite + dickite, the amount of alunite, sulphosalts and quartz correlates to large extent with *Axb* in direct and inverse manner (positive or negative contribution in the principal components). Based on these findings, iterative integrations were performed using all data points. Since it was not possible to find models that are able to predict any index, the samples were subdivided following their mineralization styles, deriving two linear equations that describe two distinguished textural domains of mineralisation - stockwork and disseminated sulphides with RMSE and R^2 of 2.5 and 0.82 respectively (Fig. 11).

Fig. 12 presents *OWi* as function of kaolinite content in the −0.150 + 0.075 mm size fraction, suggesting a strong correlation with R^2 of 0.80. Similar to the *Axb* index, the correlations shown in Fig. 12 reconfirm that kaolinite content is a key driver in grinding behaviour. An increase in kaolinite content in the sampled size fraction would imply an increase in *OWi*. One possible reason for this could be that kaolinite group minerals present plastic behaviour, leading to increased energy consumption per tonne ground ore (Spagnoli et al., 2017; Yu et al., 2016). Nevertheless, one could observe that S10 did not follow the general trend being present as an outlier which OWi value cannot be explained by kaolinite content in the sampled size fractions. This suggests that apart from kaolinite content, other ore characteristics (e.g. additional minerals, grain size, texture, etc.) may influence S10 grindability; although, it was not identified in this research.

The PCA results suggest that alunite, kaolinite + dickite and sulphosalts content correlate with *OWi*. Similar to the drop weight test results interpretation, Fig. 13 presents two equations per mineralization style which predict *OWi* values, with RMSE and R^2 of 9.08 kWh/t and 0.68 respectively. It can be inferred that the gangue mineralogy does directly affects the way the material breaks. However, textural relationships cannot be neglected, as the studied block presents high variability in terms of mineralization styles (stockwork, disseminated, massive). In addition, it was suggested to sub-divide the block into two domains in order to find any sort of correlation between the modal mineralogy and the indices. Therefore, it is assumed that the mineral content alone does not affect comminution behaviour, in contrast to the known fact that textures have a significant influence on the way the rocks break (Djordjevic, 2013; Gy et al., 1995; Vizcarra et al., 2010; Wang et al., 2015).

4. Conclusions

The current study has shown the feasibility of predicting ore behaviour in comminution through rapid methodological tests and at the same time considering ore mineralogy. The following conclusions have been drawn:

The content of kaolinite and dickite in the studied ore correlates to its resistance to impact breakage. An increase in kaolinite content correlates to an increase in *OWi* and a decrease in *Axb*. Within the domains characterized with kaolinite content above 15%, the predicted *OWi* can be expected to reach values higher than 10 kWh/t and *Axb* below 23.

The modal mineralogy based *OWi* and *Axb* could be used as a guide for optimal ore blending for downstream treatment.

Two geometallurgical domains of the block based on textural characteristics could be integrated in mine production schedule in terms of ore residence time in the grinding unit.

The information about the modal distribution of kaolinite group minerals in advanced argillic alteration would allow production control through its integration into the block model. However, the presence of minerals in low concentrations, such as rutile, brings challenges in terms of their quantification. Therefore, further research is oriented to increase the models robustness by finding the elemental expressions that better describe the studied block mineralogy.

The single particle impact breakage used in this study proved to bring a fast, reliable and low-material demanding tool for geometallurgical testing which can be applied in early-stage geometallurgical characterization projects.

Acknowledgements

The authors would like thank Dr. Simon Michaux for the support and guidance in the comminution tests methodology and modelling. Thanks go also to Dr. Hassan Bouzahzah for the automated mineralogy analysis support, and to the anonymous reviewers whose recommendations enhanced the quality of this research article.

References

Baum, W., 2014. Ore characterization, process mineralogy and lab automation a roadmap for future mining q. Miner. Eng. 60, 69–73. https://doi.org/10.1016/j.mineng.2013.11.008.

Bish, D., Plötze, M., 2011. X-ray powder diffraction with emphasis on qualitative and quantitative analysis in industrial mineralogy. Eur. Mineral. Union Notes Mineral.

Bouzahzah, H., Benzaazoua, M., Mermillod-Blondin, R., Pirard, E., 2015. A novel procedure for polished section preparation for automated mineralogy avoiding internal particle settlement. In: 12th International Congress for Applied Mineralogy (ICAM). 10–12 August 2015, Istanbul, Turkey.

Bradshaw, D.J., 2014. The role of ' process mineralogy' in improving the process performance of complex sulphide ores. XXVII IMPC, 20–24 October, Santiago de Chile, p. 24.

Bueno, M.P., Kojovic, T., Powell, M.S., Shi, F., 2013. Multi-component AG / SAG mill model. Miner. Eng. 43–44, 12–21. https://doi.org/10.1016/j.mineng.2012.06.011.

Conca, J.L., Rossman, G.R., 1985. Core softening in cavernously weathered tonalite. J. Geol. 93, 59–73.

Cropp, A., Goodall, W., Bradshaw, D., Hunt, J., Berry, R., 2014. Communicating and integrating geometallurgical data along the mining value chain. XXVII IMPC, 20–24 October, Santiago de Chile, p. 12.

Djordjevic, N., 2013. Image based modeling of rock fragmentation. Miner. Eng. 46, 68–75. https://doi.org/10.1016/j.mineng.2013.03.002.

Evans, C.L., Wightman, E.M., Manlapig, E.V., Coulter, B.L., 2011. Application of process mineralogy as a tool in sustainable processing. Miner. Eng. 24, 1242–1248. https://doi.org/10.1016/j.mineng.2011.03.017.

Graham, S., Brough, C., Cropp, A., 2015. An Introduction to ZEISS Mineralogic Mining and the correlation of light microscopy with automated mineralogy: a case study using BMS and PGM analysis of samples from a PGE- bearing chromitite prospect. In: Precious Metals'15. Falmouth, Cornwall, UK, p. 11.

Gy, O.L., Bhasin, R., Barton, N., Grimstad, E., Chryssanthakis, P., 1995. Engineering geological characterization of low strength anisotropic rocks in the Himalayan region for assessment of tunnel support. Jutogh Group Pre-Cambrian Jeori-Wangtu Gneissic Complex 40.

Keeney, L., 2010. The Development of a Novel Method for Integrating Geometallurgical Mapping and Orebody Modelling. The University of Queensland.

Keeney, L., Walters, S., 2009. Development of geometallurgical comminution mapping and modelling. In: 41st Annu. Meet. Can. Miner. Process. January 20, Ottawa, Ontario, Canada, 19p.

Koncagül, E.C., Santi, P.M., 1999. Predicting the unconfined compressive strength of the Breathitt shale using slake durability, Shore hardness and rock structural properties. Int. J. Rock Mech. Min. Sci. 36, 139–153. https://doi.org/10.1016/S0148-9062(98)00174-0.

Lishchuk, V., 2016. Geometallurgical Programs – Critical Evaluation of Applied Methods and Techniques. Luleå University of Technology.

Lishchuk, V., Lamberg, P., Lund, C., 2015. Classification of geometallurgical programs based on approach and purpose. 13th Bienn. SGA Meet Miner. Resour. a Sustain. world., vol. 4, 1431–1434.

Lopera Montoya, P.A., 2014. Geometallurgical Mapping and Mine Modelling - Comminution Studies: La Colosa Case Study, AMIRA P843A by. University of Tasmania.

Lotter, N.O., 2011. Modern Process Mineralogy: an integrated multi-disciplined approach to flowsheeting q. Miner. Eng. 24, 1229–1237. https://doi.org/10.1016/j.mineng.2011.03.004.

Lund, C., Lamberg, P., 2014. Geometallurgy – a tool for better resource efficiency. Eur. Geol. 37, 39–43.

Lynch, A., Mainza, A., Morrell, S., 2015. Ore comminution measurement techniques. In: Lynch, A. (Ed.), Comminution Handbook. The Australian Institute of Mining and Metallurgy, Carlton, Victoria, pp. 43–60.

De Magalhães, F.N., Tavares, L.M., 2014. Rapid ore breakage parameter estimation from a laboratory crushing test. Int. J. Miner. Process. 126, 49–54. https://doi.org/10.1016/j.minpro.2013.11.007.

Michaux, S., Kojovic, T., 2008. Comminution test work and modelling. In: AMIRA P843 GeM III Technical Volume 1. Hobart, Australia.

Napier-Munn, T.J., Morrell, S., Morrison, R.D., Kojovic, T., 1996. Mineral comminution circuits: their operation and optimisation. JKMRC monograph series in mining and mineral processing, second ed. Julius Kruttschnitt Mineral Research Centre,

Indooroopilly, Qld Australia.
Spagnoli, G., Sridharan, A., Oreste, P., Di Matteo, L., 2017. A probabilistic approach for the assessment of the influence of the dielectric constant of pore fluids on the liquid limit of smectite and kaolinite. Appl. Clay Sci. 145, 37–43. https://doi.org/10.1016/j.clay.2017.05.009.
Suazo, C.J., Kracht, W., Alruiz, O.M., 2010. Geometallurgical modelling of the Collahuasi flotation circuit. Miner. Eng. 23, 137–142. https://doi.org/10.1016/j.mineng.2009.11.005.
Tungpalan, K., Manlapig, E., Andrusiewicz, M., Keeney, L., Wightman, E., 2015. An integrated approach of predicting metallurgical performance relating to variability in deposit characteristics. Miner. Eng. 71, 49–54. https://doi.org/10.1016/j.mineng.2014.10.004.
Vatandoost, A., Fullagar, P., Walters, S., Kojovic, T., 2009. Towards petrophysical characterization of comminution behavior. In: 41st Annu. Meet. Can. Miner. Process. January 20, Ottawa, Ontario, Canada, 22p.
Vizcarra, T.G., Wightman, E.M., Johnson, N.W., Manlapig, E.V., 2010. The effect of breakage mechanism on the mineral liberation properties of sulphide ores. Miner. Eng. 23, 374–382. https://doi.org/10.1016/j.mineng.2009.11.012.
Walters, S., 2009. New research initiatives in geometallurgical integration moving towards a common operating language. In: 41st Annu. Meet. Can. Miner. Process. January 20, Ottawa, Ontario, Canada, 9 p.
Wang, C., Wang, H., Fu, J., Liu, Y., 2015. Flotation separation of waste plastics for recycling – a review. Waste Manag. 41, 28–38. https://doi.org/10.1016/j.wasman.2015.03.027.
Wills, B.A., Finch, J.A., 2016. Chapter 17 - Modeling and Characterization BT - Wills' Mineral Processing Technology, Eighth ed. Butterworth-Heinemann, Boston, pp. 449–462. https://doi.org/10.1016/B978-0-08-097053-0.00017-0.
Yu, C.Y., Chow, J.K., Wang, Y.-H., 2016. Pore-size changes and responses of kaolinite with different structures subject to consolidation and shearing. Eng. Geol. 202, 122–131. https://doi.org/10.1016/j.enggeo.2016.01.007.
Zhou, J., Gu, Y., 2016. Chapter 6 - Geometallurgical Characterization and Automated Mineralogy of Gold Ores. In: Adams, M.D. (Ed.), Gold Ore Processing, Second ed. Elsevier, pp. 95–111. https://doi.org/10.1016/B978-0-444-63658-4.00006-2.